Mechanics & Industry **19**, 208 (2018)
© AFM, EDP Sciences 2018
https://doi.org/10.1051/meca/2018032

Mechanics & Industry

Available online at:
www.mechanics-industry.org

REGULAR ARTICLE

CFD simulation of air effect on flow field characteristics of hydro-viscous clutch with constant speed difference

Xudong Zheng[1], Fangwei Xie[1,2,*], Diancheng Wu[1], Xinjian Guo[1], Bing Zhang[1], Van Xo Nguyen[3], and Yun Wang[1]

[1] School of Mechanical Engineering, Jiangsu University, Zhenjiang, PR China
[2] The State Key Laboratory of Fluid Power and Mechatronic Systems, Zhejiang University, Hangzhou, PR China
[3] The Institute of Mechanical and Electrical Engineering, Hanoi University of Mining and Geology, Hanoi, Vietnam

Received: 19 January 2018 / Accepted: 19 June 2018

Abstract. The purpose of this paper is to study the air effects on transmission characteristics of hydro-viscous clutch and reveal the distribution law of the flow field of the oil film. The computational-fluid-dynamics (CFD) simulation model of oil film with radial oil grooves between friction pairs is taken as the study object. Considering the air effects, the pressure field, two-phase distribution, transmission torque and temperature field of the oil film are analyzed comparatively by using the CFD technology. The results show that the presence of air changes the pressure and temperature distributions of the oil film. With increase of the absolute rotational speed, the air volume fraction increases and the radius value of the air-liquid boundary decreases under condition of constant speed difference, which makes the coverage rate of the oil film on the surface of the friction disks reduce and the transmission torque of the oil film decrease. These simulation results are attributed to the study of hydro-viscous-drive and its applications. This paper also can provide a theoretical basis for the mechanism of power transmission through oil film in the presence of air effects.

Keywords: CFD / hydro-viscous clutch / oil film / air / transmission torque

1 Introduction

Hydro-viscous clutch, based on Newton's law of viscosity, transfers the power through the viscous shear force of the oil film in the clearance between friction disk and steel disk and regulates the output speed by adjusting the oil film thickness. Hydro-viscous clutch has significant effects on soft-start, stepless speed regulation, energy saving and so on [1], so that it is widely used in the fans, pumps, belt conveyors and other large mechanical equipment.

At present, many scholars at home and abroad have studied the mechanism of hydro-viscous drive (HVD). Liu [2] revealed the effect of speed difference on HVD by using the distributed analytical method. Xiao [3] analyzed the flow pattern of the oil film between the friction pairs and found that the flow pattern is turbulent flow at high rotational speeds, which results in that the fluid lubrication between the friction pairs is insufficient. Huang [4] found that the temperature rise at high rotational speed is higher than that at low rotational speed by analyzing the heat transfer of the fluid in the gap between the HVD friction pairs. Meng and Hou [5,6] studied the multi-physical distribution, the bearing capacity and the transmission torque of the oil film during the soft-start process of the hydro-viscous clutch. Zeng et al. [7] established a fluid-solid coupling transient heat transfer model of the friction disks during the bonding process of the wet clutch, and the distribution of temperature field along the radial and circumferential directions of the friction disks was obtained. Cho [8] proposed a multi-physics model to predict oil film dynamics and found that the torque of the multi-phase flow model significantly degrades at high rotational speeds. Jammulamadaka and Gaokar [9] took into account the oil viscosity-temperature dependency, the oil surface tension and the compressibility of the air. The study shows that the oil film rupture occurs at high rotational speeds and the simulation model which considered the compressibility of the air is closer to the experiment data. Feng et al. [10,11] built the model of the oil film with double circular oil grooves and analyzed the evolution rule of the two-phase flow region based on the volume of fluid (VOF) model by considering the flow field characteristics such as oil supply, rotational speed difference, inlet temperature and the oil viscosity-temperature dependency. Takagi et al. [12] used two-phase flow model and experimental visualization measurement to study the effect of two-phase flow on drag torque in a wet clutch and found that the drag torque gradually

* e-mail: xiefangwei@ujs.edu.cn

decreased because the bubbles covered the clutch disk surface. Wu et al. [13] found that the oil mainly discharges through the groove and the air flows into the non-grooved area from the upstream side of the groove. Mahmud et al. [14] presented an improved simulation model with an extended simulation domain to consider the effect of oil inflow and outflow behavior on the drag torque. Wang et al. [15] developed a two-phase CFD model with MRF to investigate open clutch drag torque behavior.

Previous researches about HVD in the speed regulation stage are all aimed at its braking condition (that is, the passive friction disk is stationary). However, in the speed regulation stage, the passive friction disk is rotational. In this paper, the transmission torque transferred through the oil film in the speed regulation stage has been studied. Under conditions of constant speed difference, the air effects on the flow field and transmission characteristics of oil film will be analyzed comparatively based on the VOF model in ANSYS Fluent.

2 Mathematical model of HVD

2.1 Basic operating principle

The HVD, based on Newton's law of viscosity, transfers the power through the viscous shear force of the oil film in the clearance between multiple friction pairs. There is rotational speed difference between the active and the passive friction disks, so the Newtonian fluid in the gap between the friction pairs is subjected to shearing action. While transferring the power, the oil also takes away the heat produced by the shearing of the oil film.

The calculation model of the HVD torque is shown in Figure 1 [16]. The transmission torque can be obtained:

$$T = n\int_{R_1}^{R_2} 2r\mu \frac{\frac{2\pi}{60}(\omega_1-\omega_2)r}{h}\pi r dr = \frac{1}{60}n\pi\mu(\omega_1-\omega_2)\frac{1}{h}(R_2^4-R_1^4), \quad (1)$$

It can be seen from the formula that the oil film transmission torque is determined by the number of friction pairs, the dynamic viscosity, the relative rotational speed of the active and passive friction disk, the size of the inner and outer diameter of the friction disk and the thickness of the oil film.

2.2 Analysis of flow regime

According to the theory of flow around rotational disks [17], main factors that affect the flow regime in the axial direction are film thickness h, kinematic viscosity v and rotational speed ω, then a dimensionless variable is defined as

$$\zeta = h\sqrt{\frac{\omega}{v}\frac{2\pi}{60}} = h\sqrt{\frac{\pi\omega}{30v}}. \quad (2)$$

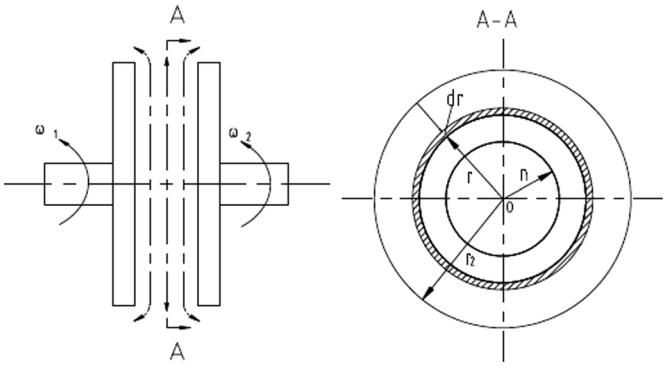

Fig. 1. Schematic diagram of torque between disks.

When the circumferential velocity of fluid reduces to 1% of tangential velocity of disks, $\zeta = 5$, a boundary layer thickness can be derived, $\delta \approx 5(30v/\pi\omega)^{0.5}$. The flow field variation occurs almost within this boundary layer. In this paper, the oil kinematic viscosity at 30 °C is $v = 23\,\mathrm{mm}^2/\mathrm{s}$ and the rotational speed is 2000 RPM, then boundary layer thickness is obtained, $\delta \approx 5(30v/\pi\omega)^{0.5} = 1.657$ mm. The oil film is completely within the fluid boundary layer. Based on the radius and the excircle tangential velocity of disks, Reynolds number is defined as

$$Re = \frac{R^2\omega}{v}, \quad (3)$$

When $\mathrm{Re} = 10^5$, $\omega = 1027.7$ RPM; when $\mathrm{Re} = 2\times10^5$, $\omega = 2055.4$ RPM.

Therefore, when the rotational speed of the active friction disk is 0–1027.7 RPM, the flow regime between the friction disks is the laminar flow; when the rotational speed is 1027.7–2055.4 RPM, the flow regime is unstable laminar flow with vortexes; when the rotational speed is higher than 2055.4 RPM, the flow regime becomes the turbulent flow.

2.3 Establishment of CFD model

The geometrical model of the fluid between the friction disks with 15 radial oil grooves is built by Solidworks software. Considering the rotational periodicity of oil film, the geometrical model is simplified and the 1/15 of the complete model is considered for CFD analysis, as shown in Figure 2. The inner circular surface is the oil inlet and the outer circular surface is the oil outlet. The grooved face is active plane and the flat face is passive plane, and both walls are assumed to be rotating. Both side surfaces are periodic boundary A and periodic boundary B, respectively. Table 1 lists the structural parameters of the fluid domain calculation model.

The simplified model is transferred to the pre-processing software ICEM for structured mesh division. Due to the smaller axial size of the model, the mesh is refined axially. In order to test the effect of meshing method on the accuracy of the calculation results, the grid independence verification has been carried out under conditions of $\omega_1 = 450$ RPM, $\omega_2 = 0$ RPM and $\mu = 0.02$ Pa s. Owing to the periodicity in the rotational direction, the meshing methods used in the circumferential direction are

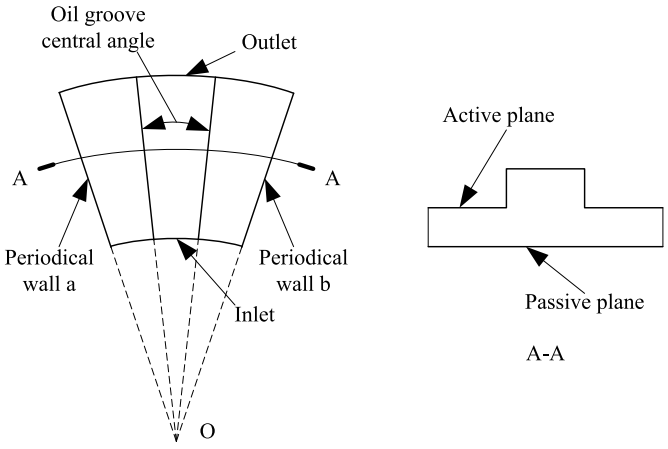

Fig. 2. Schematic diagram of the fluid domain model.

Table 1. Calculation parameters of the fluid domain model.

Parameter	Value
Outer radius (mm)	146
Inner radius (mm)	113.5
Simplified model angle (°)	24°
Film thickness (mm)	0.1
Groove depth (mm)	0.2
Groove central angle (°)	4.5

all same. Table 2 lists the results of independence verification of structural grid and shows the influence of meshing method on the maximum pressure and the output torque. The influence is very small. In order to reduce the calculation time of the computer, the No. 4 meshing method is considered as the best meshing scheme.

2.4 Boundary conditions

In ANSYS Fluent, the steady state VOF model is taken as the calculation model. Turning on the energy equation and choosing the laminar flow model. Considering the effects of air, the air is set to be the main phase (compressible) and the oil is set to be the secondary phase (incompressible). The surface tension model is turned on. The surface tension is set to 0.03 N/m and the contact angle is set to 9° [18]. The oil viscosity-temperature characteristics are neglected and the oil viscosity is set to a fixed value. Table 3 lists the properties of the lubricating oil and air.

The boundary conditions of the calculation model are set as follows: the calculation domain is fluid; the inlet boundary is set as the constant velocity inlet and its value is 0.255 m/s; the outlet boundary is set as the natural pressure outlet and its value is 0 MPa; the active and passive planes are assumed to be the rotational walls with no-slip shear. Both side surfaces are assumed to be periodic boundary.

In order to investigate the effects of the absolute rotational speed (the rotational speed of the passive friction disk) on HVD, the relative rotational speed is constant and the absolute rotational speed is variable. As shown in Table 4, from case 1 to case 6, the value of the relative rotational speed is 450 RPM constantly, while that of the absolute rotational speed is 0–1000 RPM.

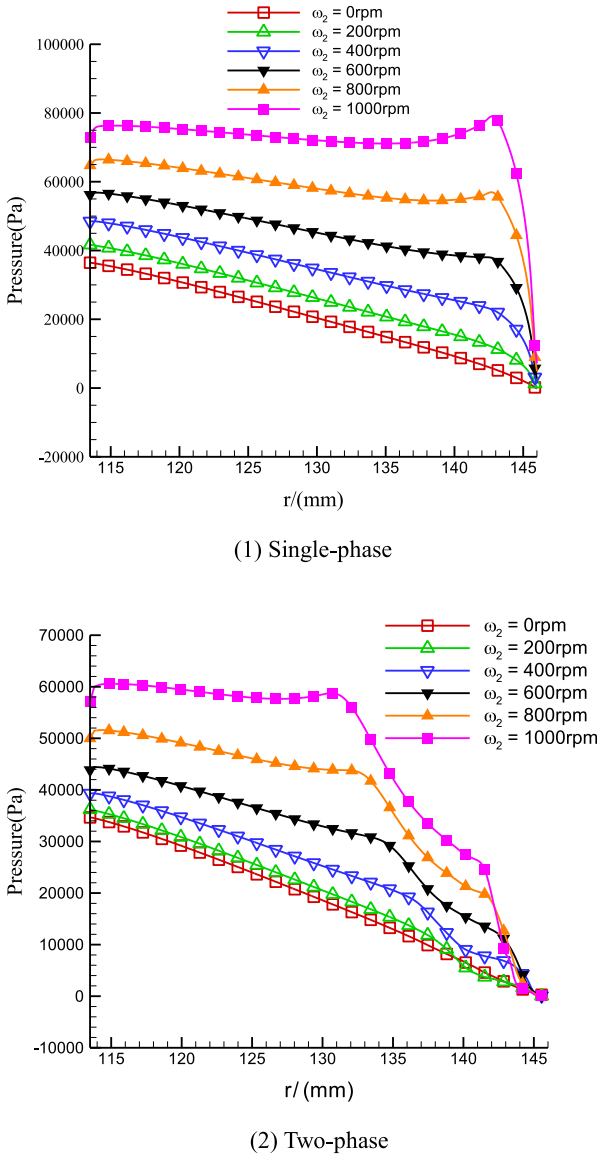

Fig. 3. The radial pressure distribution of the oil film in the groove region.

3 CFD simulation results

3.1 Pressure field distribution of oil film

Neglecting the air effect, Figure 3-(1) shows the radial oil pressure distribution in the oil groove region on cross section of $z = 0.05$ mm. From case 1 to case 6, the radial pressure in the oil groove region increases with an increase in absolute rotational speed and decreases with an increase in radius. At the same time, due to the boundary effect, the radial pressure will reduce rapidly to the natural pressure at the outer radial. Considering the air effect, Figure 3-(2) shows the radial oil pressure distribution in the

Table 2. Independence verification of structural mesh.

No.	Radial dimension (mm)	Number of circumferential layers		Number of axial layers		Number of cells	Maximum pressure (MPa)	Output torque (N m)
		Groove region	Non-groove region	Groove region	Non-groove region			
1	0.1	20	80	3	2	512146	0.1085	0.2293
2	0.1	20	80	6	2	624616	0.1079	0.2284
3	0.1	20	80	6	4	1024292	0.1077	0.2282
4	0.15	20	80	6	4	455266	0.1077	0.22815
5	0.15	20	80	9	6	682899	0.1076	0.22803
6	0.2	20	80	18	12	770993	0.1078	0.2280

Table 3. Property of lubricating oil and air.

Parameter	Oil	Air
Density (kg/m^3)	872	1.225
Specific heat (J/kg K^{-1})	2000	1006.43
Thermal conductivity (m K)	0.15	0.0242
Dynamic viscosity (Pa s)	0.02	1.7894e-5

Table 4. The parameter of cases.

Case	Input rotational speed ω_1 (RPM)	Absolute rotational speed ω_2 (RPM)	Relative rotational speed $\Delta\omega$ (RPM)
1	450	0	450
2	650	200	450
3	850	400	450
4	1050	600	450
5	1250	800	450
6	1450	1000	450

oil groove region on cross section of $z = 0.05$ mm. Compared with Figure 3-(1), the radial pressure declines. When the radius reaches a certain value, the radial pressure will reduce significantly, and the certain value of the radius decreases with increasing absolute rotational speed.

Neglecting the air effect, Figure 4-(1) shows the radial oil pressure distribution in the non-groove region on cross section of $z = 0.05$ mm. With the increase of absolute rotational speed and radius, the radial oil pressure increases rapidly at the inner radial and reaches a value which is irrelevant to the absolute rotational speed, then the radial oil pressure decreases with the increase of the radius. However, when $\omega \geq 600$ RPM, the radial oil pressure increases significantly near the outer radial, and the radial oil pressure at the outer diameter increases with the increase of the absolute rotational speed. Considering the air effect, Figure 4-(2) shows the radial oil pressure distribution in the non-groove region on cross section of $z = 0.05$ mm. Compared with Figure 4-(1), the peak value

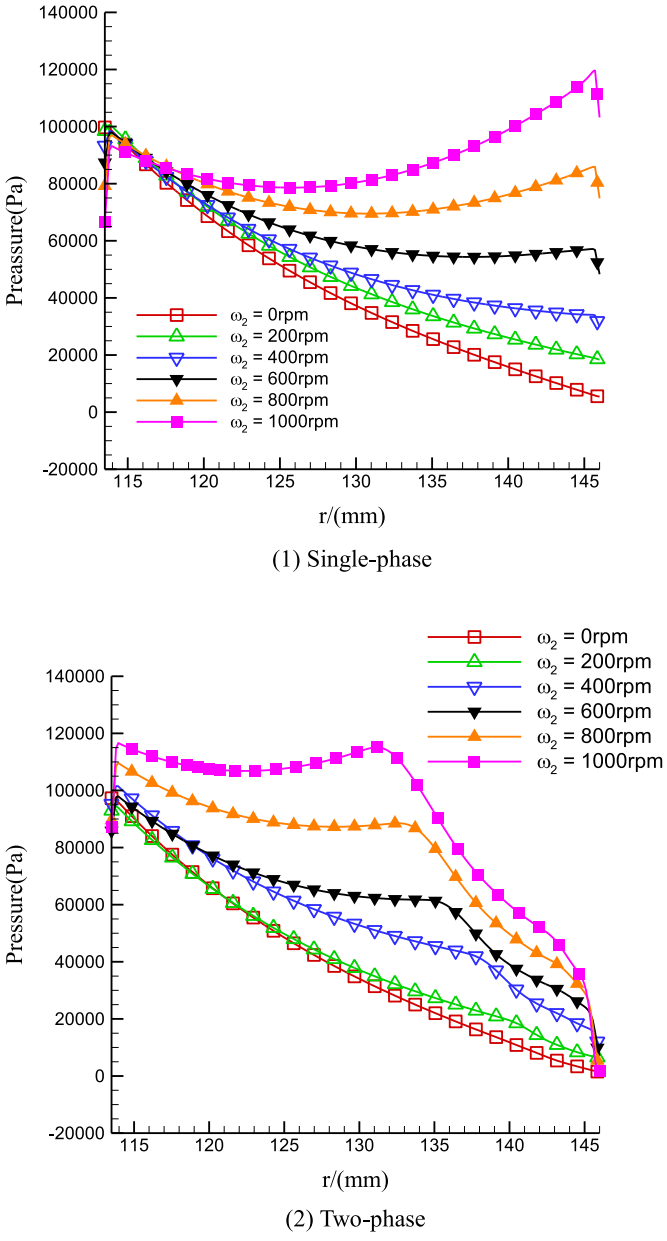

Fig. 4. The radial pressure distribution of the oil film in the non-groove region.

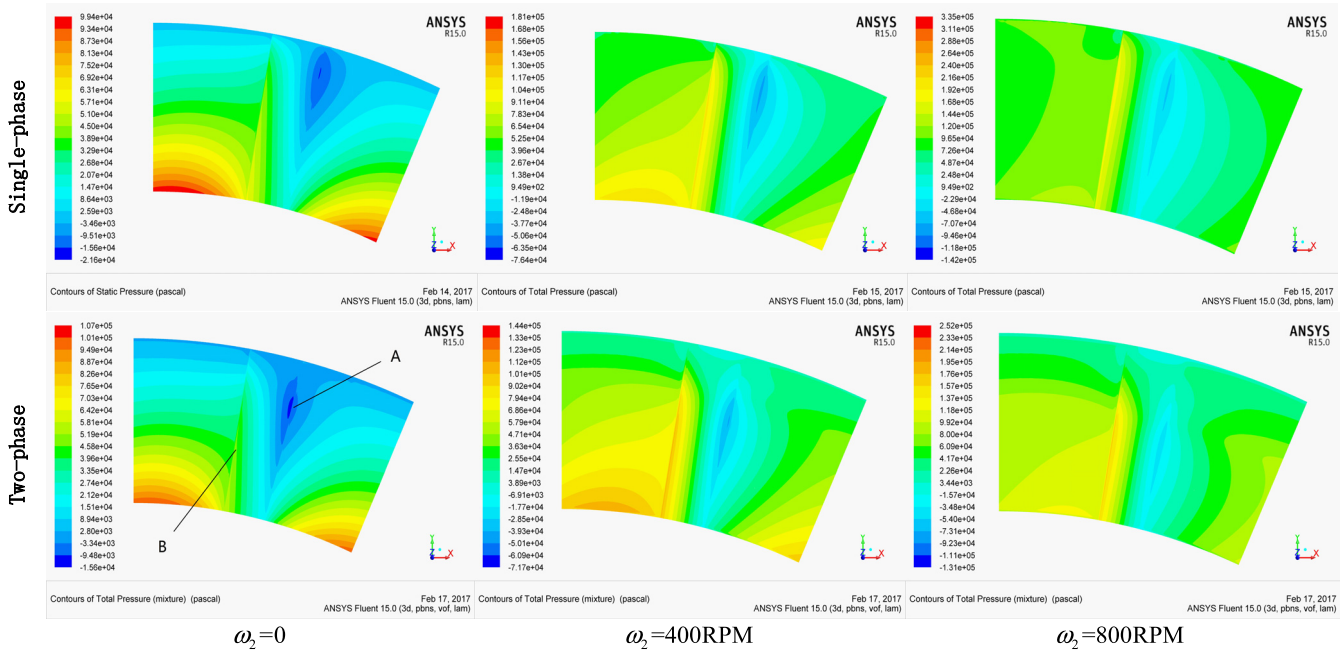

Fig. 5. The pressure distribution contour on mid-plane of $z = 0.05$ mm.

of the radial oil pressure at the inner diameter increases with the increase of the absolute rotational speed. When the radius reaches a certain value, the radial oil pressure in the non-groove region will reduce significantly, and the certain value of the radius decreases with the increase of the absolute rotational speed (Fig. 5). Figure 5 shows the contour of pressure distribution on mid-plane, which can help to understand Figs. 3 and 4.

Without taking into account the air effect, Figure 6-(1) shows the circumferential oil pressure distribution on cross section of $r = 120$ mm and $z = 0.05$ mm. With the increase of the absolute rotational speed, the total pressures in both the oil groove and non-groove regions gradually increase. There still are the high pressure and low pressure effects at the junction between the oil groove region and the non-groove region, and the maximum absolute values of high pressure and low pressure gradually increase. The increase of the maximum absolute value of low pressure results in the oil film cavitation, and the value can reduce by increasing the oil film depth. Considering the air effect, Figure 6-(2) shows the circumferential oil pressure distribution on cross section of $r = 120$ mm and $z = 0.05$ mm. Compared with Figure 6-(1), whether considering the air effect or not, it has little effect on the circumferential oil pressure distribution. The maximum absolute values of high pressure and low pressure just decline a little.

3.2 Two-phase distribution of oil film

Figure 7 shows the air volume fraction on cross section of $z = 0.05$ mm from case 1 to case 6. At the low absolute rotational speed, there will be air in the gap between the friction pairs and the air volume fraction increases gradually with the increase of the radius. The air flows mainly into the gap from the inflow side of the oil groove region and the oil flows out the gap from the outflow side of the oil groove region. The air volume fraction in the non-groove region is less than that in the oil groove region. From case 1 to case 6, the oil film coverage area (that is, the blue area in which the air volume fraction is 0) decreases gradually with the increase of the absolute rotational speed, and the oil-free area at the outer diameter of the oil groove region (that is, the red area in which the air volume fraction is 1) expands gradually due to that the gas reflux effect enhances with the increase of the absolute rotational speed.

Figure 8 shows the radial distribution of the air volume fraction in the non-groove region. The air volume fraction at the inner diameter of the non-groove region is 0. When the radius reaches a certain value, the air volume fraction begins to increase, and the certain value of the radius is defined as a turning value. From case 1 to case 6, the turning value decreases constantly, which means that the oil film coverage area decreases constantly. At the same time, the increase of the air volume fraction results in the decrease of the oil pressure, and the higher the air volume fraction is, the lower the oil pressure is.

3.3 Analysis of transmission torque

Figure 9 shows the simulation results of the transmission torque under single-phase and two-phase conditions, and the torques decreases with the increase of the absolute rotational speed under both conditions. Comparison of case 1 and case 6, in theory, the values of the transmission torques should be equal due to the same relative rotational speed, while the simulation value of case 6 is much less than that of case 1. It is surmised that, with increasing rotational speeds, the oil radial velocity near active friction disk is higher than that near passive friction disk, so the oil flows out of friction pairs along active wall and reflows into

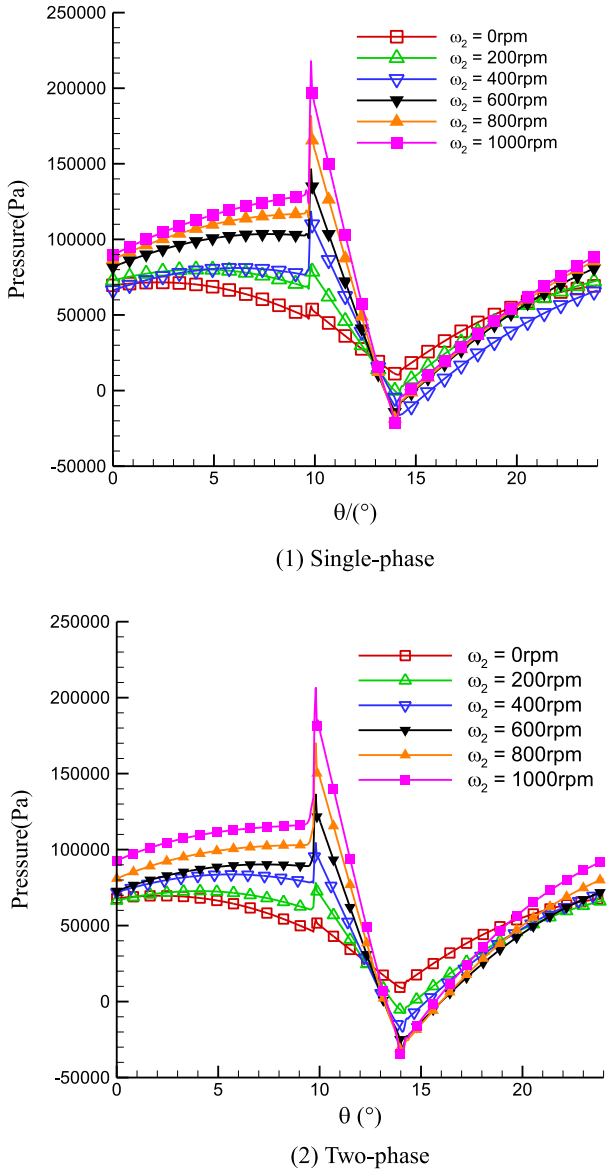

Fig. 6. The circumferential pressure distribution.

friction pairs along passive wall. The vortex phenomenon occurs and develops at outer radial locations, which may result in the drop of the transmission torque for single-phase flow.

It is obvious that the original formula of the transmission torque should be amended. In addition, the output torque of two-phase flow is always less than that of single-phase flow. The viscosity of the air is 1.7894×10^{-5} kg/(m s) and that of the lubricating oil is 0.02 kg/(m s), and the former is less than the latter. When the air flows into the gap between the friction pairs, the air volume fraction increases and the oil film coverage rate decreases, which results in the decrease of the transmission torque.

3.4 Temperature field distribution of oil film

Neglecting the air effect, Figure 10-(1) shows the radial oil temperature distribution in the oil groove region on cross section of $z = 0.05$ mm. From case 1 to case 6, the radial oil temperature distribution have the same trends that the oil temperature increase with the increase of the radius and reaches peak values near the outer diameter. The peak value of the oil temperature increases with the increase of the absolute rotational speed. Due to the boundary effect, the oil temperature will drop sharply to a fixed value, 300 K, which does not change with the change of the absolute rotational speed. In addition, the oil temperature increases with the increase of the absolute rotational speed.

Considering the air effect, Figure 10-(2) shows the radial oil temperature distribution in the oil groove region on cross section of $z = 0.05$ mm. Compared with Figure 10-(1), the radius of oil temperature peak is closer to the outer radius, and the oil temperature is higher. This indicates that the existence of the air makes the local high temperature zone occur near the outer diameter, but the oil temperature will drop rapidly to normal temperature at the outer diameter due to the larger oil film thickness and the obvious gas reflux phenomenon in the oil groove region.

Neglecting the air effect, Figure 11-(1) shows the radial oil temperature distribution in the non-groove region on cross section of $z = 0.05$ mm. The oil temperature reaches a peak value which increases with the increase of the absolute rotational speed near the outer diameter. Then the oil temperature will drop sharply to a fixed value which is slightly higher than normal temperature, 304 K.

Considering the air effect, Figure 11-(2) shows the radial oil temperature distribution in the non-groove region on cross section of $z = 0.05$ mm. Compared with Figure 11-(1), the oil temperature increase with the increase of the radius and do not drop at the outer diameter. At the outer edge of the oil film, the oil temperature reaches the maximum value. Compared with Figure 11-(2), the existence of the air makes the local high temperature zone occur near the outer diameter, but the oil temperature will rise constantly due to that the oil film thickness is small and there almost is not the obvious gas reflux phenomenon in the non-groove region.

Combining with the Figures 10 and 11, the oil temperature between the friction disks increases with the increase of the absolute rotational speed, so the transmission efficiency decreases with the increase of the absolute rotational speed and the wasted energy is translated into the heat energy, which result in a substantial rise of the oil temperature at the same point. The existence of the air makes the oil film coverage rate decrease, which results in that the transmission torque continues to decrease and more energy is translated into the heat energy. This is the reason for that the oil temperature at the outer diameter of the oil film is higher with considering the effect of the air.

Without taking into account the air effect, Figure 12-(1) shows the circumferential oil temperature distribution on cross section of $r = 145$ mm and $z = 0.05$ mm. In the case 1, the oil temperature in the oil groove region reduces directly to about 300 K. However, from case

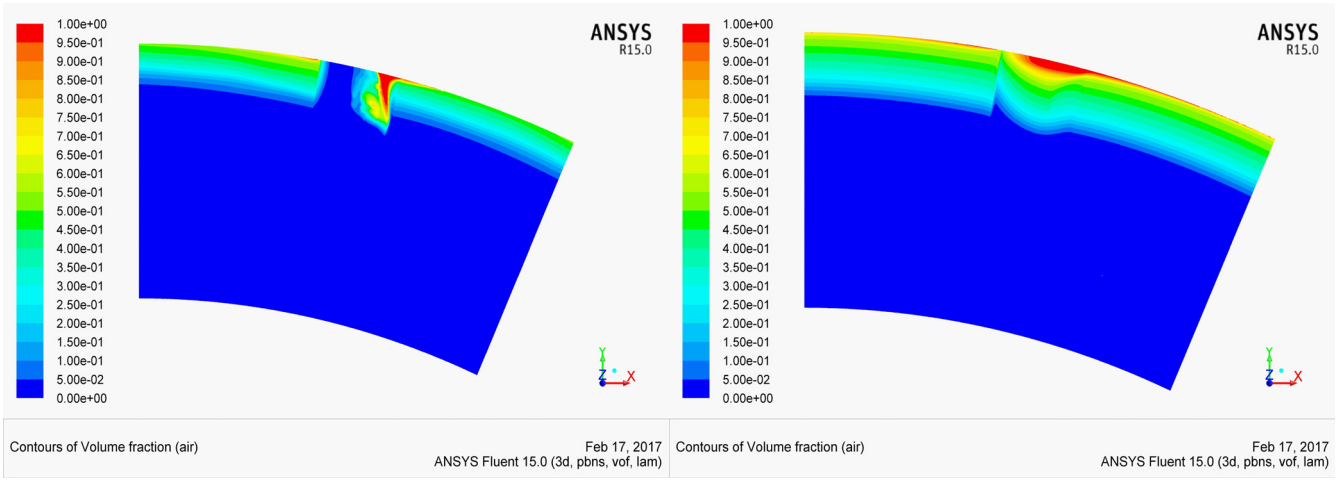

ω_2=0 ω_2=400RPM

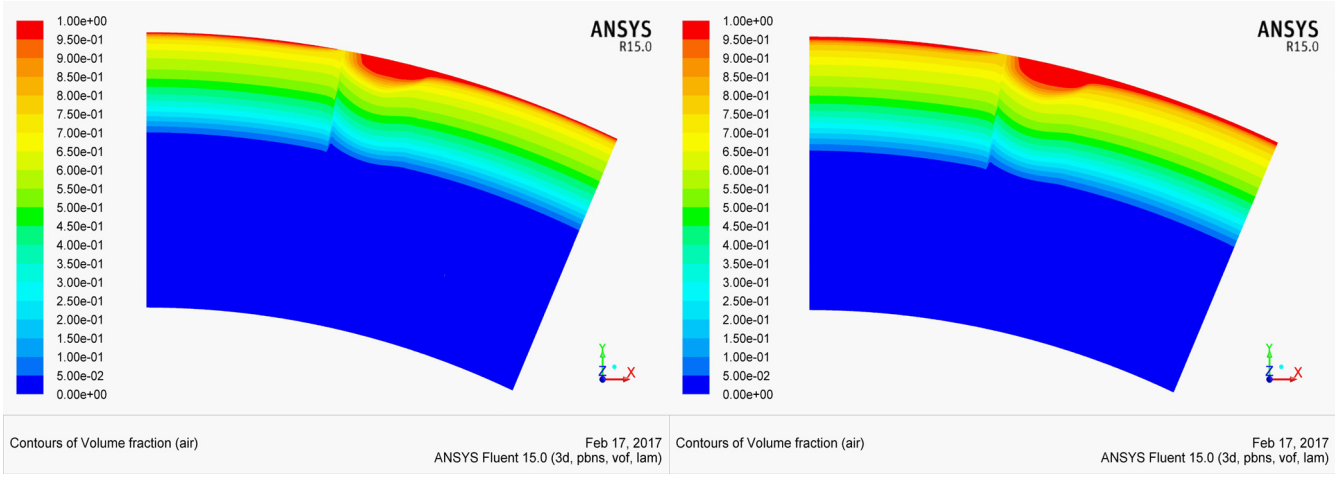

ω_2=800RPM ω_2=1000RPM

Fig. 7. The air volume fraction on cross section of $z = 0.05$ mm.

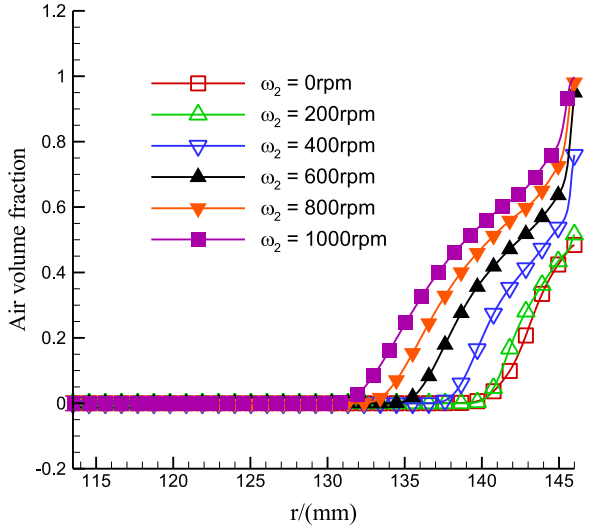

Fig. 8. The radial distribution of the air volume fraction in the non-groove region.

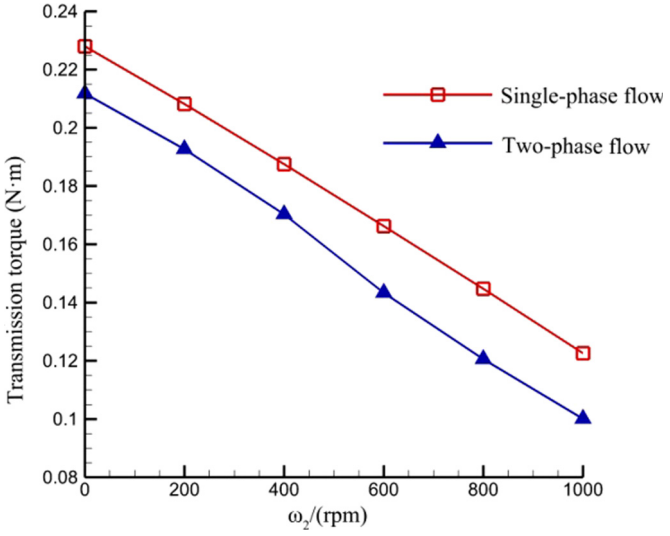

Fig. 9. The transmission torque with the absolute rotational speed.

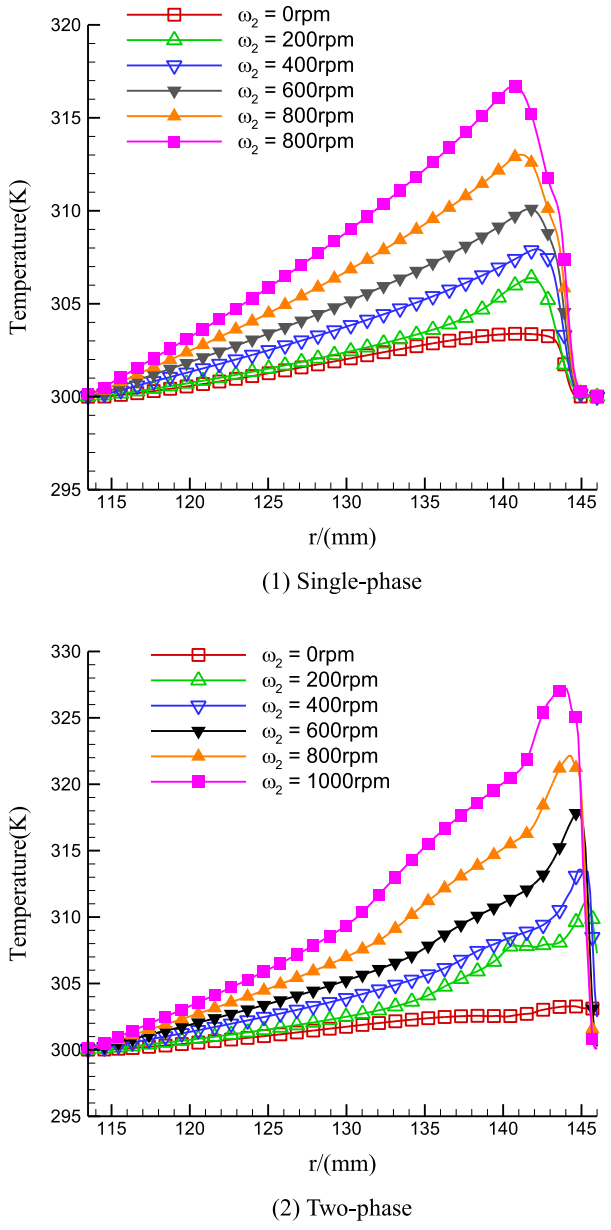

Fig. 10. The radial oil temperature distribution in the oil groove region.

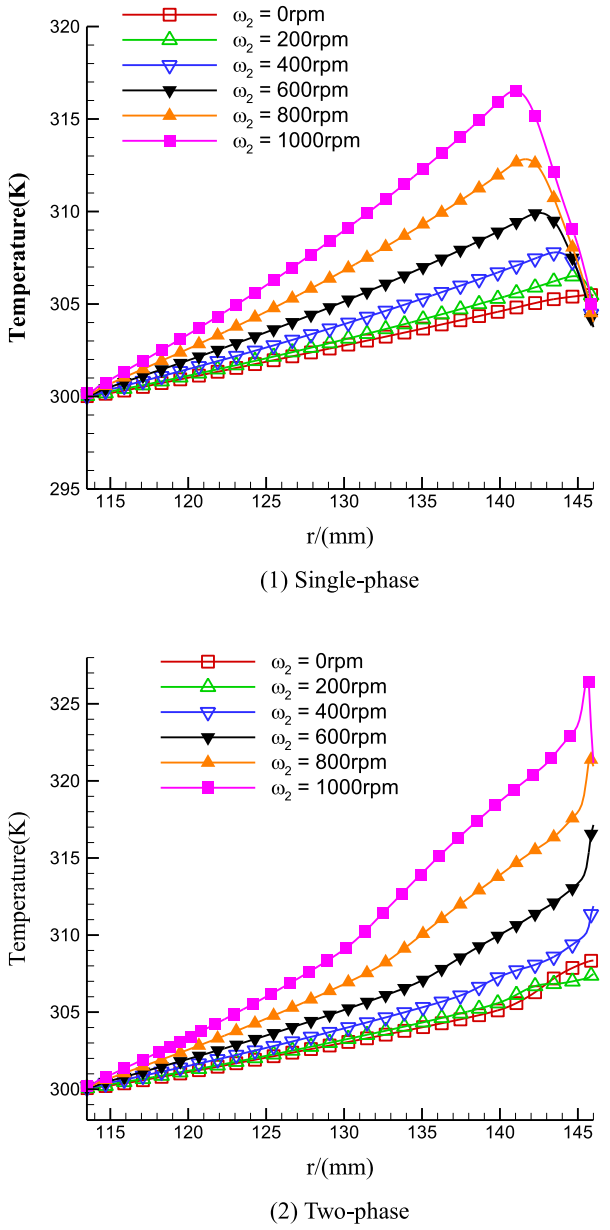

Fig. 11. The radial oil temperature distribution in the non-groove region.

2 to case 6, the oil temperature in the oil groove region will increase firstly in the outflow side of the oil groove region, and then reduces to about 300 K. In addition, the oil temperature in the outflow side increases with the increase of the absolute rotational speed.

Considering the air effect, Figure 12-(2) shows the circumferential oil temperature distribution on cross section of $r = 145$ mm and $z = 0.05$ mm. Compared with Figure 12-(1), at the same place, the oil temperature is far higher than that with neglecting the air effect, and the oil temperature distribution in the oil groove region is also different. Considering the air effect, the oil temperature in the oil groove region decreases firstly and then increases when the absolute rotational speed is 0 RPM. This is the reason for that the circumferential friction effect of the friction disks on the oil is less than the reverse pressure difference in the oil groove region, so the oil flows backwards. However, from case 2 to case 6, the circumferential friction effect of the friction disks on the oil enhances and the oil begins to flow along the circumferential direction. Therefore, the decrease of the oil temperature in the outflow side of case 1 no longer occurs. Due to the phenomenon of the air reflux at the outer diameter, the air reflux region is also local low temperature zone which will compress the original high temperature zone inward, and the compression effect is not significant at the junction of the oil groove region and non-oil region, so the oil temperature at the junction is higher than that in the oil groove region and non-groove region.

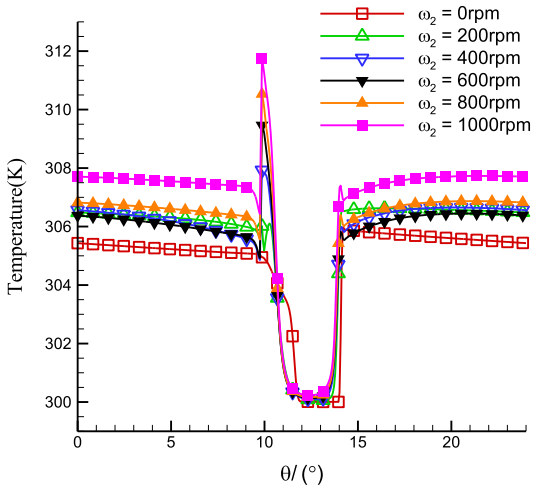

(1) Single-phase

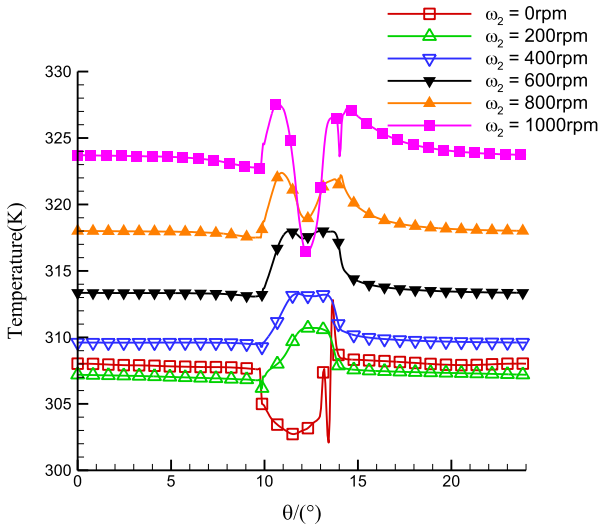

(2) Two-phase

Fig. 12. The circumferential oil temperature distribution.

4 Conclusions

In this paper, the air effects on the HVD characteristics under conditions of constant speed difference and variable rotational speed conditions were investigated. By considering the air effect, the pressure field, two-phase distribution, transmission torque and temperature field of the oil film were analyzed and compared.

The Reynolds number of the oil in the gap between the friction disks increases with the increase of the absolute rotational speed, and the flow pattern gradually changes from the laminar flow to the transition flow. The oil pressure decreases with the increase of the radius, and this trend declines with the increase of the absolute rotational speed. In addition, the oil pressure drops rapidly when the radius reaches a turning value.

The air volume fraction is 0 in the inner diameter, and the area is the complete oil film coverage area. When the radius reaches a turning value, the air volume fraction turns and begins to increase, and the value of the radius decreases with the increase of the absolute rotational speed, which means that the oil film coverage area decreases. In addition, the increase of air volume fraction results in the decrease of the oil pressure at this turning position. The higher the air volume fraction is, the lower the oil pressure is.

The existence of the air makes the oil film coverage rate decrease, which results in that the transmission torque decreases and the wasted energy is translated into the heat energy. Therefore, the oil temperature between the friction disks increases significantly. However, the oil temperature will drop rapidly at the outer diameter of the oil groove region due to the obvious gas reflux phenomenon.

Nomenclature

ρ	density, kg/m^3
μ	dynamic viscosity, Pa s
v	kinematic viscosity, mm^2/s
c	specific heat capacity, J/kg K^{-1}
T	transmission torque, N m
Re	Reynolds number
h	film thickness, mm
ω_1	rotational speed of active friction disk, RPM
ω_2	rotational speed of passive friction disk, RPM
$\Delta\omega$	relative rotational speed, RPM
R_1	inner radius of disk, mm
R_2	outer radius of disk, mm
n	number of friction pairs (number of oil film)

Acknowledgement. The authors would like to acknowledge the support of the National Natural Science Foundation of China (51675234, 51575245), and Open Foundation of the State Key Laboratory of Fluid Power and Mechatronic Systems of Zhejiang University (GZKF-201717).

References

[1] C. Wei, J. Zhao, Hydro-viscous drive technology, Defense Industry Press, Beijing, 1996
[2] Y. Liu, The study about the mechanical effects of the liquid viscous transmission oil film, Coal Mine Mach. 9 (2001) 26–28
[3] L. Xiao, Study of characteristic and experimental of the hydro-viscous drive, Theses, Shandong University of Science and Technology, 2008
[4] J. Huang, Research on the mechanism of fluid power transmission by shear stress in hydro-viscous drive, Theses, Zhejiang University, 2011
[5] Q. Meng, Y. Hou, Effects of oil film squeezing on hydro-viscous drive speed regulating start, Tribol. Int. 43 (2010) 2134–2138
[6] Q. Meng, Y. Hou, Effects of friction disk surface groove on speed-regulation start, Ind. Lubr. Tribol. 61 (2009) 325–331
[7] H. Zeng, et al., Influence of radial trapezoidal groove inclined angles on temperature distribution of wet friction disk, Lubr. Eng. 38 (2013) 14–17

[8] J. Cho, A multi-physical model for wet clutch dynamics, Theses, University of Michigan, 2012
[9] A. Jammulamadaka, P. Gaokar, Spin loss computation for open clutch using CFD, SAE Int. J. Engines 4 (2011) 1536–1544
[10] S. Feng, Study on flow transmission characteristics of hydro-viscous clutch in tracked vehicle, Theses, Beijing Institute of Technology, 2015
[11] S. Feng, S. Yao, Prediction on the fluid torque by shear stress in hydro-viscous drive with consideration of thermal effect, Chin. Hydraul. Pneum. 7 (2015) 89–95
[12] Y. Takagi, et al., Effect of two-phase flow on drag torque in a wet clutch, J. Adv. Res. Phys. 2 (2011)
[13] W. Wu, Z. Xiong, J. Hu, S. Yuan, Application of CFD to model oil-air flow in a grooved two-disc system, Int. J. Heat Mass Transf. 91 (2015) 293–301
[14] S.F. Mahmud, S.A. Pahlovy, M. Kubota, M. Ogawa, N. Takakura, Multi-phase simulation for studying the effect of different groove profiles on the drag torque characteristics of transmission wet clutch, SAE Technical Paper, 2016-01-1144, 2016
[15] P. Wang, N. Katopodes, Y. Fujii, Two-phase MRF model for wet clutch drag simulation, SAE Int. J. Engines 10 (2017) 1327–1337
[16] F. Xie, Influence law of temperature field and deformed interface on hydro-viscous drive characteristics, Theses, China University of Mining and Technology, 2010
[17] H. Schlichting, Boundary layer theory, Beijing World Publishing Corporation, Beijing, 2016
[18] H. Jibin, P. Zengxiong, W. Chao, Experimental research on drag torque for single-plate wet clutch. ASME J. Tribol. 134 (2012) 014502-1–014502-6

Cite this article as: X. Zheng, F. Xie, D. Wu, X. Guo, B. Zhang, V.X. Nguyen, Y. Wang, CFD simulation of air effect on flow field characteristics of hydro-viscous clutch with constant speed difference, Mechanics & Industry **19**, 208 (2018)